Journal of
Composites Science

MDPI

Article

Efficient and Rapid Removal of Nickel Ions from Electroplating Wastewater Using Micro-/Nanostructured Biogenic Manganese Oxide Composite

Jiaoqing Li [1,†], Li Li [2,†], Yongxuan Liu [2], Jin Liu [2] and Lin Li [2,*]

[1] Guangdong Provincial Key Laboratory of Conservation and Precision Utilization of Characteristic Agricultural Resources in Mountainous Areas, School of Life Sciences, Jiaying University, Meizhou 514015, China; lijiaoqing@jyu.edu.cn
[2] National Key Laboratory of Agricultural Microbiology, College of Life Science and Technology, Huazhong Agricultural University, Wuhan 430070, China; lily999wy@126.com (L.L.); hzaulyx@webmail.hzau.edu.cn (Y.L.); liujinlj1987@163.com (J.L.)
* Correspondence: lilin@mail.hzau.edu.cn; Tel.: +86-27-8728-6952
† These authors contributed equally to this work.

Abstract: Manganese oxides reportedly exhibit pronounced adsorption capacities for numerous heavy-metal ions owing to their unique structural properties. Herein, a biogenic manganese oxide (BMO) composite was developed and used to remove Ni ions from Ni^{2+}-containing electroplating wastewater. The formation of BMO and the micro-/nanoscale fine microstructure were characterized via scanning/high-resolution transmission electron microscopies and X-ray diffraction assays. Under the optimized conditions, with an adsorption temperature of 50 °C, pH 6, the BMO composite showed a 100% removal efficiency within a rapid equilibrium reaction time of 20 min towards an initial Ni^{2+} concentration of 10 mg L^{-1} and a remarkable removal capacity of 416.2 mg g^{-1} towards an initial Ni^{2+} concentration of 600 mg L^{-1} in Ni-electroplating wastewater. The pseudo-second-order equation was applicable to sorption data at low initial Ni^{2+} concentrations of 10–50 mg L^{-1} over the time course. Moreover, Freundlich isotherm models fitted the biosorption equilibrium data well. Fourier-transform infrared spectroscopic analysis validated that the removal capacity of the BMO composite was closely associated with structural groups. In five continuous cycles of adsorption/desorption, the BMO composite exhibited high Ni^{2+} removal and recovery capacities, thereby showing an efficient and continuous performance potential in treating Ni^{2+}-containing industrial wastewater.

Keywords: manganese oxide; electroplating wastewater; Ni^{2+}; removal

Citation: Li, J.; Li, L.; Liu, Y.; Liu, J.; Li, L. Efficient and Rapid Removal of Nickel Ions from Electroplating Wastewater Using Micro-/Nanostructured Biogenic Manganese Oxide Composite. *J. Compos. Sci.* **2024**, *8*, 63. https://doi.org/10.3390/jcs8020063

Academic Editors: Salvatore Brischetto and Chi-Hui Tsou

Received: 18 December 2023
Revised: 30 January 2024
Accepted: 4 February 2024
Published: 7 February 2024

1. Introduction

With the rapid development of the electroplating industry, the discharge of heavy metals into the environment from wastewater is becoming a serious environmental and health concern in China and other countries [1]. Electroplating heavy-metal wastewater has been mainly categorized as chromium-containing, silver-containing, copper-containing, zinc-containing, cadmium-containing, nickel-containing, etc., and, as it is commonly mixed with other metals, cyanide, and multiple acidic and alkali substances, the resulting wastewaters are the third most severe industrial pollutants worldwide [2]. In China, electroplating wastewater has an average annual volume of 2.7 billion gallons [3], with nickel concentrations in the range of tens to thousands of milligrams per liter [4,5], and has become a significant and intractable environmental issue in terms of managing hazardous substances and resource recycling. Various physicochemical and biological methods, such as membrane filtration, chemical precipitation, ion exchange, chemical oxidation and reduction, electroplating, and removal by biomasses generated by naturally occurring or genetically modified microorganisms [6–8], have been developed to treat electroplating

wastewaters. Due to its economic feasibility and easy performance, adsorption is generally recognized as one of the most promising treatments for reducing heavy-metal ions from the aqueous phase.

Manganese (Mn) is one of the most abundant transition metal elements on Earth. Mn oxides are widely distributed as a common mineral in various soils, aquatic environments, and lake and marine sediments [9]. According to the oxidative pathways in natural systems, Mn oxides can be divided into biological Mn oxides (BMOs) and chemical Mn oxides (CMOs), with various BMOs being formed via biogenic Mn^{2+} oxidation mediated by certain microorganisms that harbor Mn oxidases; this method dominates the biomineralization of Mn oxides in the natural environment [10,11]. Owing to the unique structural and physicochemical properties of Mn oxides, such as their high ionic valence state and porous surface, they are potential adsorbents for heavy-metal ions. The metal-adsorption capability of the CMO-based birnessite for multiple transition metals has been evaluated [12–14], and various BMOs have also been used to adsorb heavy-metal ions, including Cu^{2+}, Zn^{2+}, Ni^{2+}, Ag^{+}, and Pb^{2+}, in previous studies [15–18]. In principle, these Mn oxide-based treatments provide additional technical approaches for heavy-metal adsorption. BMOs can be easily produced by manganese-oxidizing bacteria (MOB) and are generally recognized to have a low crystallinity and a higher specific surface area, higher electronegativity, and more pores than CMOs and are likely to have higher removal capacity for heavy metals [10,11,19]. BMOs can adsorb a variety of heavy metals, thereby controlling their migration and transformation in the environment. This capability holds significant importance and offers vast prospects for environmental restoration in contaminated areas.

In this study, we utilized a micro-/nanostructured BMO composite formed by a wild-type Mn^{2+}-oxidizing *Pseudomonas* sp. MB04B bacterium as an adsorptive material to remove Ni ions from real electroplating wastewater with a high load of Ni^{2+} and other hazardous substances, with the aim of providing a facile, efficient, and recycled biosorbent for removing Ni ions in industrial Ni-electroplating wastewater. We prepared the BMO composite via prolonged culturing of MB04B cells under the supplement of a low concentration of Mn^{2+} and characterized the multiple-phase composition and fine microstructure of the BMO by X-ray diffraction (XRD), scanning electron microscopy (SEM), and high-resolution transmission electron microscopy (HRTEM). Following the optimization of the factors affecting Ni^{2+} removal, such as temperature, pH, removal time, and initial Ni^{2+} concentration, we determined the Ni^{2+}-biosorption kinetics, analyzed the biosorption data using the Langmuir and Freundlich isotherm models, and applied the prepared BMO composite in treating the real Ni^{2+}-containing electroplating wastewater. Finally, we investigated the Ni^{2+} removal and recovery efficiency in five continuous cycles of adsorption and desorption and analyzed the corresponding band groups of the BMO composite that were involved in Ni^{2+} binding using Fourier-transform infrared (FTIR) spectroscopy.

2. Materials and Methods

2.1. Reagents

The wastewater used in this study was sampled from the raw industrial Ni-electroplating wastewater of an electroplating plant in Xiamen, Fujian Province, China, with an initial Ni^{2+} content of 5262.9 mg L^{-1}, a total phosphorus content of 35,170.9 mg L^{-1}, and a total chemical oxygen demand (COD) of 30,332.2 mg L^{-1} (Supplementary Figure S1). The wastewater was routinely stored at 4 °C and diluted to certain concentrations with deionized water for removal experiments when appropriate. Other chemicals and bacterial medium components were purchased from Sinopharm Chemical Reagent Co. Ltd. (Wuhan, China) or Aladdin (Shanghai, China) and were used as received.

2.2. Manganese Oxidation Activity Determination

A wild-type *Pseudomonas* sp. MB04B bacterium was used to prepare the BMO composite under a laboratory trial. Cells were routinely cultured in Lept media [20] at 28 °C. The

Mn^{2+}-oxidizing activity (i.e., the Mn oxide concentration formed by bacterial cells) of cell cultures that were incubated in 100 mL Lept broth (containing 1 mmol L^{-1} Mn^{2+}) over a time course of 10 days was determined according to a previously described method.

2.3. Preparation of the BMO Composite

The overnight-cultured MB04B cells were inoculated into 200 mL Lept medium supplemented with 1 mmol L^{-1} Mn^{2+} at 1% (v/v) inoculum size for culturing at 28 °C for 48 h. The formed BMO/bacteria aggregates were centrifuged at 10,000 rpm for 10 min, dried by freeze drying, and stored at 4 °C until use.

2.4. Characterization of the BMO

SEM (JSM-6390/LV, NTC, Tokyo, Japan) was used to observe the surface morphology of the as-prepared BMO. An HRTEM (JEM-2100F, JEOL, Tokyo, Japan), equipped with an energy-dispersive spectroscopy detector, was used to investigate the microstructure of the BMO sample and analyze its elements. The HRTEM was operated at an acceleration voltage of 200 kV, and sample preparation and HRTEM observation were performed following the manufacturer's manual. The crystal structure of the BMO was determined by an XRD spectrometer (Bruker D8 Advance X, Billerica, MA, USA) as previously described [21]. The crystal size was calculated by the software Jade 5.0. X-ray photoelectron spectroscopy (XPS) analysis of the BMO was conducted using an XPS spectrometer (VG Multilab 2000, Thermo Scientific, Waltham, MA, USA) with an Al Kα X-ray source (1486 eV) and a base pressure of 3×10^{-9} Torr in the analytical chamber, following a previous protocol [22].

2.5. Adsorption Experiments

The biosorption experiments were performed in a 100 mL Erlenmeyer flask with a load of 40 mg (dry weight) BMO composite unless otherwise specified. In the removal capacity and the removal equilibrium experiments, the raw Ni-electroplating wastewater was diluted to a series of dilutions of 10, 50, 100, 200, 400, and 600 mg L^{-1}. In the second-order kinetic analysis and isotherm fitting experiments, the removal was conducted at 50 °C and 200 rpm shaking for 60 min. After removal, the mixtures were centrifugated at 10,000 rpm for 10 min and Ni^{2+} contents of the liquid supernatants were determined. The mixture without adding the BMO composite was set as the negative control.

A quantity of 10 mg L^{-1} Ni-electroplating wastewater was used in the adsorption/desorption cycle experiments. After removal, the biosorbents were harvested via centrifugation (10,000 rpm for 10 min) and then added into 10 mL of 0.1 mol L^{-1} HCl and shaken at 60 rpm for 30 min for the desorption of Ni^{2+} ions from the BMO composite in each cycle. The HCl-treated BMO composite was washed with deionized water to neutral pH for further use in each cycle.

2.6. Kinetics and Isotherm Analysis

In all adsorption experiments, the residual Ni^{2+} ion content was determined using an atomic absorption spectrophotometer (HITACHI 180-80, Tokyo, Japan). The residual Ni^{2+} content was used to calculate the absolute removal rate and removal capacity of Ni^{2+} in various wastewater dilutions using the following equations:

$$\text{Removalrate}\ (\%) = \frac{C_i - C_e}{C_i} \times 100\% \quad (1)$$

$$q_e(\text{mgg}^{-1}) = \frac{C_i - C_e}{M} \quad (2)$$

where C_i denotes the initial Ni^{2+} ion concentration (mg L^{-1}), C_e denotes the equilibrium Ni^{2+} concentration (mg L^{-1}), and M denotes the mass concentration (g L^{-1}) of the BMO composite.

2.7. FTIR Spectroscopy

The FTIR spectra of the BMO composite before and after Ni^{2+} ion adsorption were analyzed using an FTIR spectrometer (Spectrum One, Perkin-Elmer, Waltham, MA, USA). All FTIR spectra were recorded within the 400–4000 cm^{-1} range. Samples were prepared as previously described [22].

2.8. Data Analysis

Graphs were prepared using Origin 11 software (Origin Lab Corp., Northampton, MA, USA). Data are presented as the average ± standard deviation (±SD) of at least three repeated experiments. Statistical analyses were conducted based on an analysis of variance (ANOVA) with the SPSS statistical software package (Version 19.0; SPSS, Inc., Chicago, IL, USA). Means were separated and compared using Fisher's protected least significant difference test.

3. Results and Discussion

3.1. Characterization of the BMO Aggregate Composite Formed by Mn^{2+}-Oxidizing Pseudomonas sp. MB04B

We previously isolated a wild-type bacterium from a Fe–Mn nodule surrounding soil [23], which was preliminarily identified as *Pseudomonas* sp. MB04B. MB04B cells were subjected to continuous 1 mmol L^{-1} Mn^{2+} enrichment in a laboratory shake-flask trial for 10 days to investigate the Mn^{2+}-activity profile of this strain. The MB04B cultures exhibited a sharp increase in Mn^{2+} activity after 24 h incubation and steadily maintained high activity across days 1–10 (Figure 1A). Interestingly, after 48 h incubation of the MB04B cells, irregular microspherical aggregates with diameters of approximately 5–7 µm were observed via SEM, and the bacteria attached to and embedded in the aggregates could be easily distinguished (Figure 1B). The XRD profile of the formed BMO (Figure 1C) revealed two characteristic diffraction peaks at 2θ of 37° (311) and 65° (440), which are consistent with the standard diffraction peaks of natural ramsdellite MnO_2 (JCPDS card no. 42-11698) [24]. Therefore, these results confirmed the pronounced Mn^{2+}-oxidizing activity of the BMOs mainly comprising ramsdellite (MnO_2).

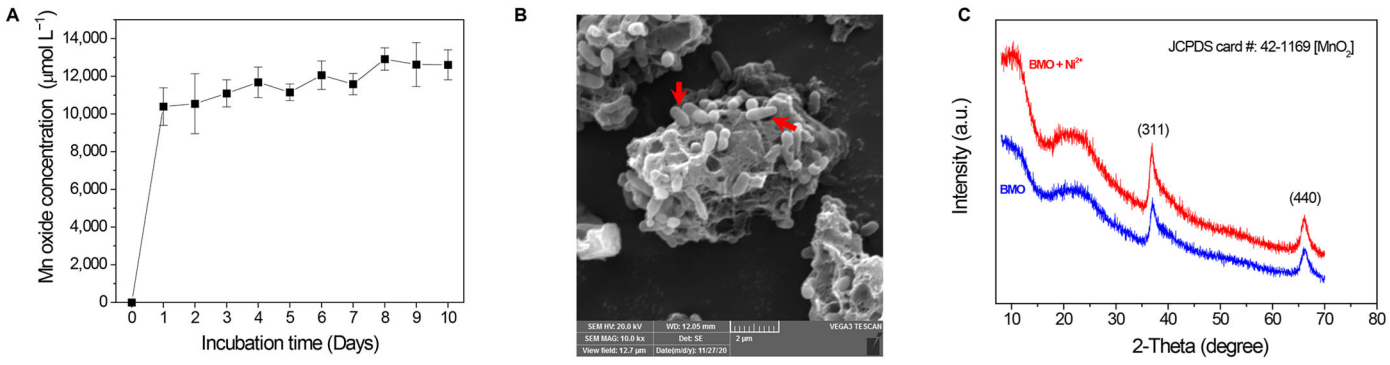

Figure 1. (**A**) Mn^{2+}-oxidizing activity curve of the BMO cultures of *Pseudomonas* sp. MB04B; (**B**) SEM micrograph of the formed aggregates at 48 h; (**C**) XRD pattern of Mn oxides of the BMO aggregates. In (**B**), red arrows indicate the attached or embedded MB04 cells.

HRTEM was performed to investigate the fine microstructure of the formed BMO aggregates. Figure 2A shows the irregular microspherical structure of a randomly observed single aggregate particle. Quantities of nanocrystalline particles with diameters of 5 ± 1 nm were dispersed and embedded in the organic matter (Figure 2A, indicated by red arrows). The lattice fringe of 0.206 nm corresponded to the *d* value of the (401) plane-spacing in the ramsdellite-type MnO_2, suggesting that the BMO aggregates formed by bacterial mineralization were micro-/nanostructure-type composites (Figure 2B). Given the

presence of porous surface and lattice vacancies that are apparently conducive to metal-ion removal [25–27], we further investigated the potential of this composite with respect to Ni^{2+} removal performance.

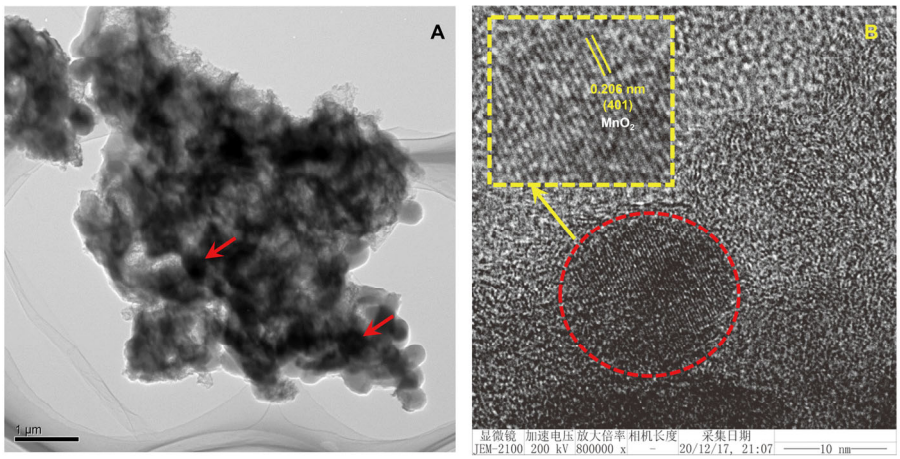

Figure 2. (**A**) HRTEM micrograph of a representative BMO aggregate particle; (**B**) measured lattice spacings of the micro-/nanostructured BMO aggregate matter.

3.2. Ni^{2+} Removal Capacity of the Composite

The industrial-grade raw Ni-electroplating wastewater used in this study contains complex and multicomponent toxic substances. In addition to a high content of Ni^{2+}, it includes a high content of total-P, multiple cyanides, and acidic and alkaline substances and a high load of COD (Supplementary Figure S1), making it extremely hazardous wastewater that cannot be discharged directly. To evaluate the Ni^{2+} biosorption capacity of the BMO composite with respect to the Ni-electroplating wastewater, an orthogonal test at four factors/three levels (Supplementary Table S1), based on temperature (30 °C, 40 °C, and 50 °C), pH (4, 5, and 6), removal time (10, 30, and 50 min), and initial Ni^{2+} concentration (10, 50, and 100 mg L^{-1}) in shake-flask incubation, was performed to optimize the adsorptive reaction conditions. As shown in Table 1, these four factors exhibited pronounced effects on the Ni^{2+} removal capacity of the BMO composite, with an effective degree order of "initial Ni^{2+} concentration > temperature > pH > removal time". The ANOVA analysis (Supplementary Table S2) also validated the significant effects of these factors. The optimized Ni^{2+}-biosorption conditions can be defined as follows: temperature of 50 °C, pH value of 6, removal time of 50 min, and initial nickel ion concentration of 10 mg L^{-1}.

Table 1. Significance analysis of the factors in the L9-orthogonal test of Ni removal efficiency.

Levels	Factors			
	Temperature (°C) Mean	pH Mean	Adsorption Time (min) Mean	Initial Ni^{2+} Concentration (mg L^{-1}) Mean
R1	34.55	37.03	38.01	94.82
R2	42.45	40.67	40.31	17.25
R3	42.57	41.87	41.24	7.50
R_j [a]	8.01	4.84	3.23	87.32
Rank	2	3	4	1

[a] Range of the corresponding values for each factor.

3.3. Adsorption Kinetics

The optimum biosorption conditions (50 °C, pH 6, and 50 min for saturated adsorption) were applied to identify the biosorption kinetics of the BMO composite in Ni^{2+} biosorption

at the varying initial Ni^{2+} concentrations of 10, 50, 100, 200, 400, and 600 mg L^{-1}. Figure 3 shows that the adsorption equilibrium reaction was rapidly conducted for 40 min for all treatments, even for only 20 min for several biosorption reactions (i.e., 10–200 mg L^{-1} Ni^{2+}). In addition, with the increase in the initial Ni^{2+} concentration, the removal capacity of Ni^{2+} also significantly increased in parallel, i.e., a maximum Ni^{2+} biosorption capacity of 416.2 mg g^{-1} was obtained under the optimized conditions for 600 mg L^{-1} of initial Ni^{2+} concentration.

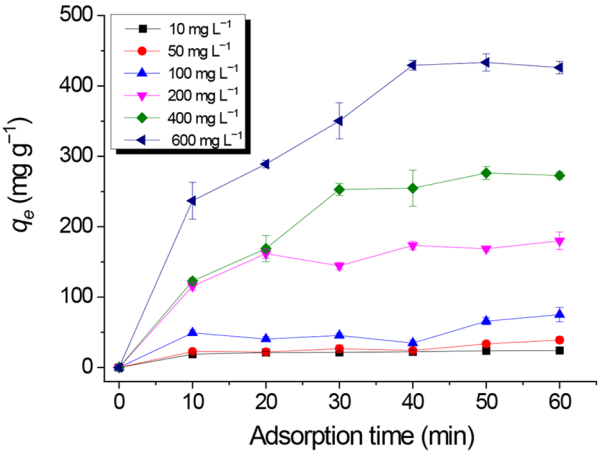

Figure 3. Biosorption equilibrium curves for manganese oxide aggregates with different initial Ni^{2+} concentrations.

The pseudo-second-order removal kinetic equation was used to test the fitting of the removal data over the time course. Lagergren's pseudo-second-order equation based on removal equilibrium capacity is generally defined as follows [28]:

$$\frac{dq_t}{dt} = k_2(q_e - q_t)^2 \quad (3)$$

and a linearized equation can be expressed by integrating Equation (3):

$$\frac{t}{q_t} = \frac{1}{k_2 q_e^2} + \frac{t}{q_e} \quad (4)$$

in Equations (3) and (4), k_2 is the secondary removal rate constant (g mg^{-1} min^{-1}) and q_e and q_t denote the removal capacity at the sorption equilibrium and time t, respectively.

Table 2 shows the profiles of the time-course sorption data fitted using Equation (3) or (4). It shows that the corresponding k_2 constant and the equilibrium removal capacity, q_e, increase following the increase in initial Ni^{2+} concentration, and the removal kinetics can be described using the pseudo-second-order model at a 10–50 mg L^{-1} initial Ni^{2+} concentration ($R^2 > 0.9$).

Table 2. Fitting parameters of pseudo-second-order kinetics.

C_0 (mg L^{-1})	Equation	R^2	k_2 (g mg^{-1} min^{-1})	q_e (mg g^{-1})
10	y = 0.03896x + 0.1755	0.9955	0.008647	25.67
50	y = 0.021x + 0.38555	0.9024	0.001144	47.62
100	y = 0.01075x + 0.21767	0.7915	0.000531	93.02
200	y = 0.00347x + 0.06935	0.8185	0.000174	288.18
400	y = 0.00215x + 0.04812	0.8811	0.000096	465.12
600	y = 0.00112x + 0.07375	0.6934	0.000017	892.86

3.4. Isotherm Equation Fitting

The Langmuir and Freundlich models were applied to analyze the removal data with different initial Ni^{2+} concentrations. The Langmuir model linearization equation [7] can be expressed as:

$$\frac{1}{Q_e} = \frac{1}{Q_{\max}} + \frac{1}{K_s Q_e C_e} \quad (5)$$

where Q_e is the removal capacity at the equilibrium of the sorbent (mg g^{-1}), Q_{max} (mg g^{-1}) is the maximum removal capacity of the sorbent (mg g^{-1}), C_e (mg L^{-1}) is the equilibrium concentration of Ni ions in solution, and K_s is the saturation constant (mg L^{-1}).

The Freundlich model linearization equation can be expressed as:

$$\ln Q_e = \ln K_f + \frac{1}{n} \ln C_e \quad (6)$$

where Q_e and C_e are the same parameters indicated above, and K_f and n are Freundlich constants denoting the removal capacity and removal intensity, respectively.

Figure 4 shows that Ni^{2+} biosorption by the BMO composite is better fitted by the Freundlich isotherm model (with the parameter of R^2 = 0.96) than the Langmuir model (R^2 = 0.84). These results suggest that the Ni^{2+} removal of the BMO composite in Ni-electroplating wastewater is a multiphase chemical removal process, which is consistent with the intrinsic structural features of the BMO composite possessing multiple surface charge groups and a layered and porous surface [29]. This multiphased biosorption is conducive to a greater sorption capacity than single-layer removal under only one level.

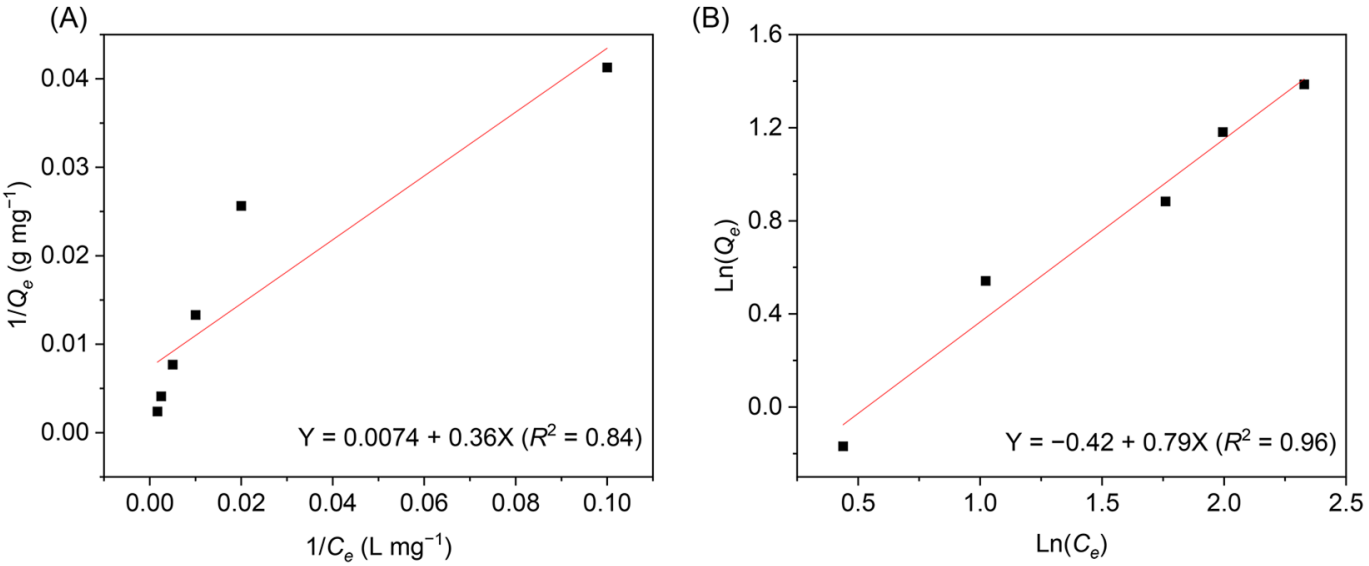

Figure 4. The Langmuir (**A**)/Freundlich (**B**) isotherm plots of the BMO composite's Ni^{2+} biosorption in the electroplating wastewater.

3.5. Characterization of Removal Using FTIR and XRD Assays

FTIR spectroscopic analyses of the BMO composite before and after Ni^{2+} removal were performed to verify the chemical groups involved in the binding of Ni ions. Figure 5 shows similar spectra for both, in which the displayed peaks at 3400–3800 cm^{-1} represent the stretching vibration peak of free –OH [30] and the peak at 2900 cm^{-1} represents the C–H (e.g., CH_3) stretching vibration peak, while the peak at 1300–1600 cm^{-1} represents the bending vibration of the –OH [31] and the varied –OH wavenumbers at 1384 cm^{-1} to 1403 cm^{-1} before and after Ni^{2+} removal are likely due to electrostatic interaction [32]. The peak at 1021.23 cm^{-1} represents the bending vibration of Mn–OH on the surface of the BMO, in addition to the characteristic vibration peaks of relatively weak Mn–O bonds in

the range of 500–700 cm^{-1}, thereby proving that Mn–O bonds exist in the BMO [33]. It is noteworthy that the BMO composite also includes Mn(II)-oxidizing cells and extracellular polymeric substances and thus has abundant anionic carboxyl and hydroxyl functional groups that might participate in Ni ion removal [34]. Moreover, the BMO composite is structurally layered and generally contains varying amounts of Mn(III) and vacant sites in the Mn layers [35], and the significant variation in the Mn–O bond wavenumbers before and after Ni^{2+} removal indicates that the Mn–O bond also plays a specific role in the Ni^{2+} removal process of the BMO composite.

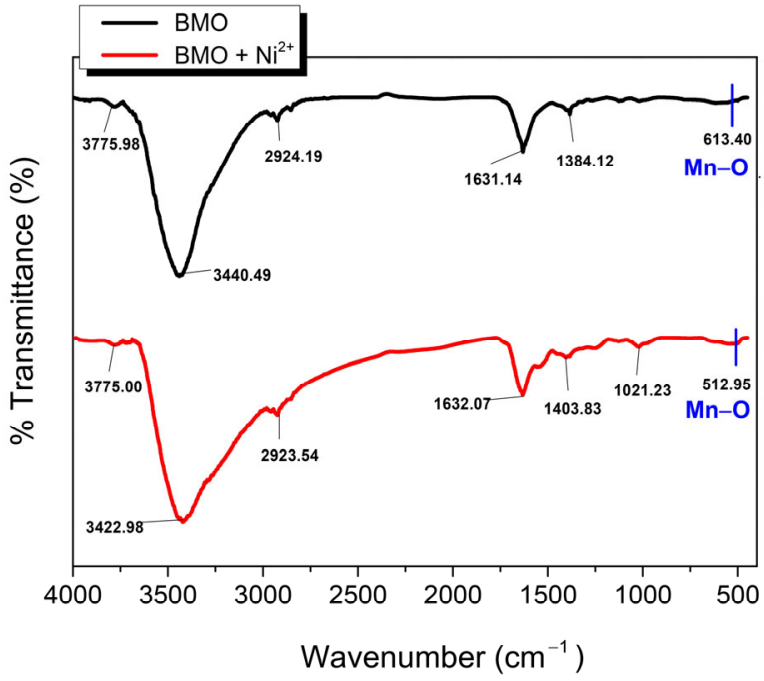

Figure 5. FTIR spectra of the BMO composite before and after Ni^{2+} removal.

XPS assays were performed to compare the varied valence states and the proportions of Mn and Ni in the BMO before and after Ni^{2+} removal. Figure 6 shows that the BMO contained different valence forms consisting of mainly Mn^{2+}, Mn^{3+}, and Mn^{4+}, and the proportion of Mn oxides in all three valent states changed significantly before and after Ni^{2+} removal, especially the ratio of Mn^{2+} in the Mn element, which increased by approximately 15% (Supplementary Table S3). Moreover, 4.39% of Ni^{3+} in the Ni element appeared in the BMO after Ni^{2+} removal (Supplementary Table S4). It has been revealed that the BMO was able to oxidize many organic compounds and metals as a pronounced oxidant in the natural environment [35]. The potential difference between the low potential of Ni^{2+} and certain organic matters (such as malic acid, tartaric acid, and citric acid, which contributed to the COD content) in electroplating wastewater and the high potential in the BMO composite-derived electron transfer between Mn^{3+}/Mn^{4+} and Mn^{2+} may increase the amount of Mn^{2+} via Mn reduction reaction [36]. Therefore, we presume that the removal of Ni ions by the BMO composite occurred not only via adsorption but also via Ni^{2+} oxidation.

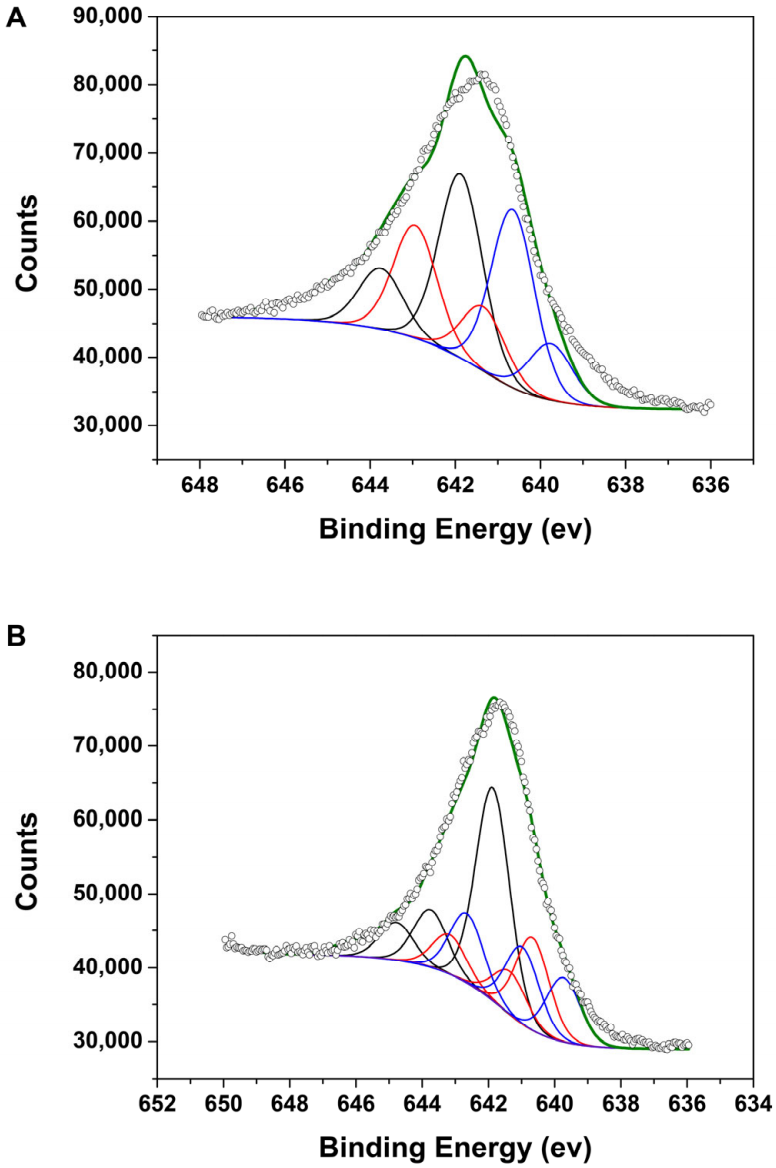

Figure 6. XPS patterns of Mn ($2p_{3/2}$) spectrograms of the BMO composite before (**A**) and after (**B**) Ni^{2+} removal. In A/B, the upper circles represent observed data. The upper thick olive curves indicate the best fit of the data. The black curves represent Mn^{4+} multiplet peaks, the red curves represent Mn^{3+}, the blue curves represent Mn^{2+}.

3.6. Ni^{2+} Adsorption/Desorption Cycles

To investigate the reusability of the BMO composite with respect to its continuous performance in treating Ni-electroplating wastewater, its Ni^{2+} adsorption and desorption efficiency was determined through five cycles of adsorption and desorption. Figure 7 shows that relatively high Ni^{2+} adsorption/desorption capacities were retained in a total of five cycles, with adsorption efficiencies of 98.1%, 94.6%, 84.5%, and 71.5% in cycles 2–5 (cycle 1 was set as 100%), respectively, and comparable recovery efficiencies (the ratio of desorption/adsorption in each cycle) of 86.7%, 85.7%, 84.0%, 71.2%, and 71.8% in cycles 1–5, respectively. The results indicate that the BMO composite can be reused in continuous adsorption/desorption operations to treat industrial wastewater containing Ni^{2+}.

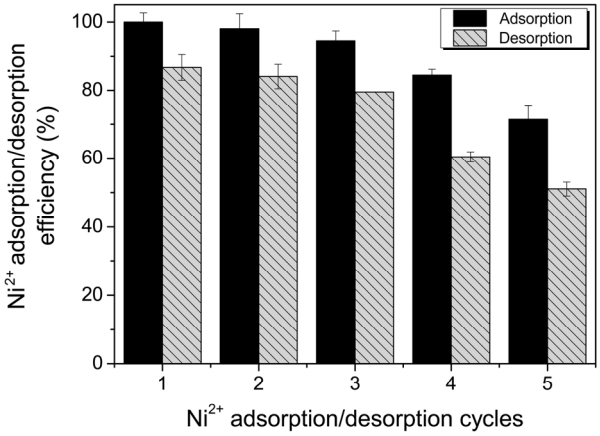

Figure 7. Ni^{2+} adsorption/desorption capacity of the BMO composite under continuously repeated operations.

Numerous studies have reported the efficient removal of heavy metals from wastewater using abiotic or biotic masses consisting of naturally occurring or recombinant microorganisms [37,38]. Several previously described systems exhibited higher levels of Ni^{2+} removal, with a maximum removal capacity of 411.8 mg g^{-1} (Table 3). In comparison, the highest Ni^{2+} removal capacity of the BMO composite prepared in this study was 416.2 mg g^{-1} at the initial Ni^{2+} concentration of 600 mg L^{-1}, a slightly higher capacity than the available biosorbents with the highest levels, thereby suggesting a comparable high absolute Ni^{2+} removal capacity for the BMO composite. The nickel electroplating wastewater used in this study contained Ni^{2+}, P (mainly phosphite and hypophosphite), and COD (malic acid, tartaric acid, and citric acid) (pH 3.0). To achieve the standard of safe discharge, we designed the following processing steps that will be studied in the future: (1) recovery of nickel by multistage cycles of adsorption using the BMO composite at pH 6.0; (2) addition of CaO to remove P, a pH > 5.0 promoting this process; and (3) microbial treatment to remove COD, with neutral pH as the optimum.

Table 3. Comparison of the maximum Ni^{2+}-removal capacities of different materials in this work and previous reports.

Removal Materials		Ni Wastewater						
Name	**Mass**	**Volume**	**Concentration**	**pH**	**Removal Capacity**	**Removal Rate**	**Equilibrium Time**	**References**
Pseudomonas sp. biomass	1.25 g [a]	100 mL	80 mg L^{-1}	4.5	336.8 mg g^{-1} [b]	–	40 min	[39]
K. oxytoca J7 EPS	20–200 mg	5 mL	10 mg L^{-1}	7.2	269.97 mg g^{-1} [b]	–	60 min	[34]
Bacillus cereus M^{1}_{16} biomass	0.1 g	50 mL	25–1100 mg L^{-1}	7.0	344.80 mg g^{-1} [b]	–	60 min	[40]
Bentonite/GO	50 mg	100 mL	100–500 mg L^{-1}	6.0	402.5 mg g^{-1} [b]	–	60 min	[41]
PVP-SiO_2	10 mg	50 mL	10–200 mg L^{-1}	5.0	46.1 mg g^{-1} [b]	–	30 min	[42]
PEC SC_1-SC_4	100 mg	200 mL	600 mg L^{-1}	7.0	411.8 mg g^{-1}	34.3%	240 min	[43]
Phosphorylated wood	50 mg	50 mL	20–200 mg L^{-1}	6.0	130.2 mg g^{-1} [b]	–	6 h	[44]
BMO	40 mg	100 mL	10 mg L^{-1} 600 mg L^{-1}	6.0	24.2 mg g^{-1} 416.2 mg g^{-1}	100% 28.6%	20 min 40 min	This study

[a] Wet weight. [b] The maximum removal capacity. EPS, exopolysaccharides.

To the best of our knowledge, the present study is the first attempt to use a bacterial BMO composite to treat raw industrial Ni-electroplating wastewater. It is worth noting that the current BMO composite exhibited relative easiness and cost-effectiveness of preparation under mild bacterial culture conditions, effectively removing Ni ions in Ni-electroplating wastewater, especially at low concentrations, and repeatable performance in treating elec-

troplating wastewater. However, modifying the surface ion charges and pore sizes is thought to be definitely conducive to a more efficient and coordinated adsorptive capacity of this system. Thus, the development of capacity-promoted BMO-biosorption systems is now one of our primary research goals.

4. Conclusions

The current study demonstrated, for the first time, that the BMO composite formed using an Mn^{2+}-oxidizing bacterium efficiently and rapidly removed Ni^{2+} ions from industrial Ni-electroplating wastewater. The adsorption equilibrium was conducted for 20 min towards an initial concentration of 10 mg L^{-1} Ni^{2+} ions, and the highest removal capacity of 416.2 mg g^{-1} was conducted under optimized conditions towards an initial concentration of 600 mg L^{-1} Ni^{2+} ions. FTIR and XPS showed that the Ni removal by the BMO composite was not only contributed by adsorption via hydroxyl and carboxyl groups and Mn-O bands, but was also contributed by Mn(III)/Mn(IV) oxidation. In addition, the engineered BMO composite exhibited efficient and feasible Ni^{2+}-removal/-recycling performance in five continuous adsorption/desorption cycle operations. Therefore, further development of this BMO material could be especially valuable for large-scale or continuous biosorption processes in treating industrial electroplating wastewater.

Supplementary Materials: The following supporting information can be downloaded at: https://www.mdpi.com/article/10.3390/jcs8020063/s1, Figure S1: A raw industrial Ni-electroplating wastewater sample of an electroplating plant in Xiamen, Fujian Province, China; Table S1: L9-orthogonal test of Ni^{2+} removal efficiency by the BMO composite biosorbent; Table S2: Analysis of variance for selected factorial model; Table S3: Mn (2p3/2) peak parameters for *Pseudomonas* sp. MB04B BMO before and after Ni^{2+} removal; Table S4: Ni (2p3/2) peak parameters for *Pseudomonas* sp. MB04B BMO after Ni^{2+} removal.

Author Contributions: Conceptualization, L.L. (Lin Li), and J.L. (Jiaoqing Li); methodology, J.L. (Jiaoqing Li), L.L. (Li Li), and J.L. (Jin Liu); formal analysis, J.L. (Jiaoqing Li), L.L. (Li Li), and Y.L.; investigation, J.L. (Jiaoqing Li), L.L. (Li Li), Y.L. and J.L. (Jin Liu); writing—original draft preparation, J.L. (Jiaoqing Li), and L.L. (Li Li); writing—review and editing, L.L. (Lin Li); supervision, L.L. (Lin Li). All authors have read and agreed to the published version of the manuscript.

Funding: This work was funded by a grant from Meizhou City's 2021 Guangdong Provincial Rural Revitalization Strategy Special Fund (grant no. 2021A0305002) that was issued to Jiaoqing Li and Lin Li, and a grant from the National Natural Science Foundation of China to Lin Li (grant no. 32170124).

Data Availability Statement: The authors confirm that the data supporting the findings of this study are available within the article or its Supplementary Materials.

Conflicts of Interest: The authors declare no conflicts of interest.

References

1. Li, S.; Dai, M.; Wu, Y.; Fu, H.; Hou, X.; Peng, C.; Luo, H. Resource utilization of electroplating wastewater: Obstacles and solutions. *Environ. Sci. Water Res. Technol.* **2022**, *8*, 484–509. [CrossRef]
2. Rajoria, S.; Vashishtha, M.; Sangal, V.K. Treatment of electroplating industry wastewater: A review on the various techniques. *Environ. Sci. Pollut. Res.* **2022**, *29*, 72196–72246. [CrossRef]
3. Huang, Z.; Hwang, J.; Huang, C.; Shi, Y. Electroplating Wastewater Treatment in China. *Miner. Met. Mater. Ser.* **2021**, *4*, 225–232. [CrossRef]
4. Wang, S.; Zhang, D.; Wang, W.; Zhong, J.; Feng, K.; Wu, Z.; Du, B.; He, J.; Li, Z.; He, L.; et al. Grave-to-cradle upcycling of Ni from electroplating wastewater to photothermal CO_2 catalysis. *Nat. Commun.* **2022**, *13*, 5305. [CrossRef]
5. Noman, E.; Al-Gheethi, A.; Saphira Radin Mohamed, R.M.; Al-Sahari, M.; Hossain, M.S.; Vo, D.-V.N.; Naushad, M. Sustainable approaches for nickel removal from wastewater using bacterial biomass and nanocomposite adsorbents: A review. *Chemosphere* **2022**, *291*, 132862. [CrossRef] [PubMed]
6. Li, H.; Chen, Y.; Long, J.; Jiang, D.; Liu, J.; Li, S.; Qi, J.; Zhang, P.; Wang, J.; Gong, J.; et al. Simultaneous removal of thallium and chloride from a highly saline industrial wastewater using modified anion exchange resins. *J. Hazard. Mater.* **2017**, *333*, 179–185. [CrossRef]
7. Wu, Y.; Li, W.; Sparks, D.L. Effect of iron(II) on arsenic sequestration by δ-MnO_2: Desorption studies using stirred-flow experiments and X-Ray absorption fine structure spectroscopy. *Environ. Sci. Technol.* **2015**, *49*, 13360–13368. [CrossRef]

8. Fu, X.-Z.; Yang, Y.-R.; Liu, T.; Guo, Z.-Y.; Li, C.-X.; Li, H.-Y.; Cui, K.-P.; Li, W.-W. Biological upcycling of nickel and sulfate as electrocatalyst from electroplating wastewater. *Water Res.* **2024**, *250*, 121063. [CrossRef] [PubMed]
9. Ding, H.; Li, Y.; Li, Y.; Liu, F.; Liu, Y.; Lu, A.; Wang, C.; Ye, H.; Zhuang, Z. The photogeochemical cycle of Mn oxides on the Earth's surface. *Mineral. Mag.* **2021**, *85*, 22–38. [CrossRef]
10. Zhou, H.; Fu, C. Manganese-oxidizing microbes and biogenic manganese oxides: Characterization, Mn(II) oxidation mechanism and environmental relevance. *Rev. Environ. Sci. Biotechnol.* **2020**, *19*, 489–507. [CrossRef]
11. Cai, Y.; Yang, K.; Qiu, C.; Bi, Y.; Tian, B.; Bi, X. A review of manganese-oxidizing bacteria (MnOB): Applications, future concerns, and challenges. *Int. J. Environ. Res. Public Health* **2023**, *20*, 1272. [CrossRef]
12. Peacock, C.L.; Sherman, D.M. Sorption of Ni by birnessite: Equilibrium controls on Ni in seawater. *Chem. Geol.* **2007**, *238*, 94–106. [CrossRef]
13. Pena, J.; Bargar, J.R.; Sposito, G. Copper sorption by the edge surfaces of synthetic birnessite nanoparticles. *Chem. Geol.* **2015**, *396*, 196–207. [CrossRef]
14. Yang, P.; Post, J.E.; Wang, Q.; Xu, W.; Geiss, R.; McCurdy, P.R.; Zhu, M. Metal adsorption controls stability of layered manganese oxides. *Environ. Sci. Technol.* **2019**, *53*, 7453–7462. [CrossRef] [PubMed]
15. Kim, E.J.; Lee, C.S.; Chang, Y.Y.; Chang, Y.S. Hierarchically structured manganese oxide-coated magnetic nanocomposites for the efficient removal of heavy metal ions from aqueous systems. *ACS Appl. Mater. Interfaces* **2013**, *5*, 9628–9634. [CrossRef] [PubMed]
16. Kim, E.-J.; Kim, J.; Choi, S.C.; Chang, Y.S. Sorption behavior of heavy metals on poorly crystalline manganese oxides: Roles of water conditions and light. *Environ. Sci. Proc. Impacts* **2014**, *16*, 1519–1525. [CrossRef] [PubMed]
17. Pei, Y.; Chen, X.; Xiong, D.; Liao, S.; Wang, G. Removal and recovery of toxic silver ion using deep-sea bacterial generated biogenic manganese oxides. *PLoS ONE* **2013**, *8*, e81627. [CrossRef] [PubMed]
18. Wan, W.; Xing, Y.; Qin, X.; Li, X.; Liu, S.; Luo, X.; Huang, Q.; Chen, W. A manganese-oxidizing bacterial consortium and its biogenic Mn oxides for dye decolorization and heavy metal adsorption. *Chemosphere* **2020**, *253*, 126627. [CrossRef] [PubMed]
19. Huang, Y.; Huangfu, X.; Ma, C.; Liu, Z. Sequestration and oxidation of heavy metals mediated by Mn(II) oxidizing microorganisms in the aquatic environment. *Chemosphere* **2023**, *329*, 138594. [CrossRef] [PubMed]
20. Krumbein, W.E.; Altmann, H.J. A new method for the detection and enumeration of manganese oxidizing and reducing microorganisms. *Helgol. Wiss. Meeresunters* **1973**, *25*, 347–356. [CrossRef]
21. Wei, S.; Wang, W.; Xiao, F. Biological oxidation of manganese mediated by the fungus *Neoroussoella solani* MnF107. *Int. J. Mol. Sci.* **2023**, *24*, 17093. [CrossRef]
22. Bai, Y.; Su, J.; Wen, Q.; Li, G.; Xue, L.; Huang, T. Removal of tetracycline by denitrifying Mn(II)-oxidizing bacterium *Pseudomonas* sp. H117 and biomaterials (BMO and MBMO): Efficiency and mechanisms. *Bioresour. Technol.* **2020**, *312*, 123565. [CrossRef]
23. Yang, W.; Zhang, Z.; Zhang, Z.; Chen, H.; Liu, J.; Ali, M.; Liu, F.; Li, L. Population structure of manganese-oxidizing bacteria in stratified soils and properties of manganese oxide aggregates under manganese-complex medium enrichment. *PLoS ONE* **2013**, *8*, e73778. [CrossRef] [PubMed]
24. Lee, S.Y.; Park, S.J. Li ion adsorption behaviors of Ni-loaded Li-Mn oxide composites. *RSC Adv.* **2014**, *4*, 21899–21903. [CrossRef]
25. Li, Y.; Ye, D.; Liu, W.; Shi, B.; Guo, R.; Pei, H.; Xie, J. A three-dimensional core-shell nanostructured composite of polypyrrole wrapped MnO_2/reduced graphene oxide/carbon nanotube for high performance lithium ion batteries. *J. Colloid Interface Sci.* **2017**, *493*, 241–248. [CrossRef] [PubMed]
26. Yin, H.; Liu, F.; Feng, X.; Liu, M.; Tan, W.; Qiu, G. Co^{2+}-exchange mechanism of birnessite and its application for the removal of Pb^{2+} and As(III). *J. Hazard. Mater.* **2011**, *196*, 318–326. [CrossRef] [PubMed]
27. Zhu, M.; Ginder-Vogel, M.; Parikh, S.J.; Feng, X.H.; Sparks, D.L. Cation effects on the layer structure of biogenic Mn-oxides. *Environ. Sci. Technol.* **2010**, *44*, 4465–4471. [CrossRef] [PubMed]
28. Ferancová, A.; Hattuniemi, M.K.; Sesay, A.M.; Räty, J.P.; Virtanen, V.T. Complexation of Ni(II) by dimethylglyoxime for rapid removal and monitoring of Ni(II) in water. *Mine Water Environ.* **2017**, *36*, 273–282. [CrossRef]
29. Peng, L.; Zeng, Q.; Tie, B.; Lei, M.; Yang, J.; Luo, S.; Song, Z. Manganese Dioxide nanosheet suspension: A novel absorbent for Cadmium(II) contamination in waterbody. *J. Colloid Interface Sci.* **2015**, *456*, 108–115. [CrossRef] [PubMed]
30. Raj, B.G.S.; Asiri, A.M.; Qusti, A.H.; Wu, J.J.; Anandan, S. Sonochemically synthesized MnO_2 nanoparticles as electrode material for supercapacitors. *Ultrason. Sonochem.* **2014**, *21*, 1933–1938. [CrossRef]
31. Jiang, R.; Huang, T.; Liu, J.; Zhuang, J.; Yu, A. A novel method to prepare nanostructured manganese dioxide and its electrochemical properties as a supercapacitor electrode. *Electrochim. Acta* **2009**, *54*, 3047–3052. [CrossRef]
32. Wan, S.; Ma, M.; Lv, L.; Qian, L.; Xu, S.; Xue, Y.; Ma, Z. Selective capture of thallium(I) ion from aqueous solutions by amorphous hydrous manganese dioxide. *Chem. Eng. J.* **2014**, *239*, 200–206. [CrossRef]
33. Omid, H.; Oghabian, M.A.; Ahmadi, R.; Shahbazi, N.; Hosseini, H.R.M.; Shanehsazzadeh, S.; Zangeneh, R.N. Synthesizing and staining manganese oxide nanoparticles for cytotoxicity and cellular uptake investigation. *Biochim. Biophys. Acta (BBA)-Gen. Subj.* **2014**, *1840*, 428–433. [CrossRef] [PubMed]
34. Ljubic, V.; Perendija, J.; Cvetkovic, S.; Rogan, J.; Trivunac, K.; Stojanovic, M.; Popovic, M. Removal of Ni^{2+} ions from contaminated water by new exopolysaccharide extracted from *K. oxytoca* J7 as biosorbent. *J. Polym. Environ.* **2023**. [CrossRef]
35. Zhu, M.; Ginder-Vogel, M.; Sparks, D.L. Ni(II) sorption on biogenic Mn-oxides with varying Mn octahedral layer structure. *Environ. Sci. Technol.* **2010**, *44*, 4472–4478. [CrossRef] [PubMed]

36. Gong, Y.; Gai, L.; Tang, J.; Fu, J.; Wang, Q.; Zeng, E.Y. Reduction of Cr(VI) in simulated groundwater by FeS-coated iron magnetic nanoparticles. *Sci. Total Environ.* **2017**, *595*, 743–751. [CrossRef] [PubMed]
37. Vijayaraghavan, K.; Yun, Y.S. Bacterial biosorbents and biosorption. *Biotechnol. Adv.* **2008**, *26*, 266–291. [CrossRef] [PubMed]
38. Wang, J.; Chen, C. Biosorbents for heavy metals removal and their future. *Biotechnol. Adv.* **2009**, *27*, 195–226. [CrossRef] [PubMed]
39. Zhang, J.; Yang, K.; Wang, H.; Lv, B.; Ma, F. Biosorption of copper and nickel ions using *Pseudomonas* sp. in single and binary metal systems. *Desalination Water Treat.* **2016**, *57*, 2799–2808. [CrossRef]
40. Naskar, A.; Guha, A.K.; Mukherjee, M.; Ray, L. Adsorption of nickel onto *Bacillus cereus* M116: A mechanistic approach. *Sep. Sci. Technol.* **2016**, *51*, 427–438. [CrossRef]
41. Chang, Y.S.; Au, P.I.; Mubarak, N.M.; Khalid, M.; Jagadish, P.; Walvekar, R.; Abdullah, E.C. Adsorption of Cu(II) and Ni(II) ions from wastewater onto bentonite and bentonite/GO composite. *Environ. Sci. Pollut. Res.* **2020**, *27*, 33270–33296. [CrossRef] [PubMed]
42. Betiha, M.A.; Moustafa, Y.M.; Mansour, A.S.; Rafik, E.; El-Shahat, M.F. Nontoxic polyvinylpyrrolidone-propylmethacrylate-silica nanocomposite for efficient adsorption of lead, copper, and nickel cations from contaminated wastewater. *J. Mol. Liq.* **2020**, *314*, 113656. [CrossRef]
43. Hu, X.; Yan, L.; Wang, Y.; Xu, M. Smart and functional polyelectrolyte complex hydrogel composed of salecan and chitosan lactate as superadsorbent for decontamination of nickel ions. *Int. J. Biol. Macromol.* **2020**, *165*, 1852–1861. [CrossRef] [PubMed]
44. Huo, H.; Yu, Y.; Zhang, X.; Tang, M.; Chen, C.; Wang, S.; Min, D. Phosphorylated wood designed as a biosorbent for effectively removing Ni^{2+} from wastewater. *Ind. Crops Prod.* **2022**, *188*, 115727. [CrossRef]